

PLASMA BETA DEPENDENCE OF THE ION-SCALE SPECTRAL BREAK OF SOLAR WIND TURBULENCE:
HIGH-RESOLUTION 2D HYBRID SIMULATIONSLUCA FRANCI^{1,2}, SIMONE LANDI^{1,3}, LORENZO MATTEINI⁴, ANDREA VERDINI⁵, PETR HELLINGER⁶(Dated: February 21, 2022)
Draft version February 21, 2022

ABSTRACT

We investigate properties of the ion-scale spectral break of solar wind turbulence by means of two-dimensional high-resolution hybrid particle-in-cell simulations. We impose an initial ambient magnetic field perpendicular to the simulation box and add a spectrum of in-plane, large-scale, magnetic and kinetic fluctuations. We perform a set of simulations with different values of the plasma β , distributed over three orders of magnitude, from 0.01 to 10. In all the cases, once turbulence is fully developed, we observe a power-law spectrum of the fluctuating magnetic field on large scales (in the inertial range) with a spectral index close to $-5/3$, while in the sub-ion range we observe another power-law spectrum with a spectral index systematically varying with β (from around -3.6 for small values to around -2.9 for large ones). The two ranges are separated by a spectral break around ion scales. The length scale at which this transition occurs is found to be proportional to the ion inertial length, d_i , for $\beta \ll 1$ and to the ion gyroradius, $\rho_i = d_i \sqrt{\beta}$, for $\beta \gg 1$, i.e., to the larger between the two scales in both the extreme regimes. For intermediate cases, i.e., $\beta \sim 1$, a combination of the two scales is involved. We infer an empiric relation for the dependency of the spectral break on β that provides a good fit over the whole range of values. We compare our results with in situ observations in the solar wind and suggest possible explanations for such a behavior.

Subject headings: plasmas — solar wind — turbulence

1. INTRODUCTION

The solar wind is an exceptional laboratory for plasma astrophysics thanks to spacecraft in situ observations. One of the best established observational results is a ubiquitous presence of a broadband range of electromagnetic fluctuations interpreted as a turbulent cascade connecting the fluid motion on large scales to small-scale kinetic fluctuations at particle scales (Bruno & Carbone 2013). At large scales, turbulent fluctuations exhibit properties consistent with magnetohydrodynamics (MHD) turbulence (e.g., Bavassano et al. 1982; Marsch & Tu 1990; Grappin et al. 1990). Approaching particle characteristic scales, a transition to a different, kinetic, regime of the turbulence is observed. This regime is characterized by a steepening of the magnetic field spectrum, followed by a further steepening at electron scales (Alexandrova et al. 2009; Sahraoui et al. 2013). A clear change in the magnetic field spectral slope is observed between the MHD and the sub-ion range (e.g., Leamon et al. 1998; Bruno et al. 2014; Lion et al. 2016), going from a Kolmogorov-like scaling with a spectral index of $-5/3$ to a steeper power law, phenomenologically consistent with a spread of the spectral index around a typical value of -2.8 .

In the solar wind, the transition between MHD and kinetic turbulence occurs close to the convected characteristic ion scales, namely the ion inertial length, d_i , and the ion Larmor radius, ρ_i . However, it is not straightforward to conclude from observations which of the two scales (or what kind of their combination) is associated to the spectral change and, consequently, which are the physical processes governing the transition and the cascade at sub-ion scales. The main reason is that the two scales are very close to each other under typical solar wind conditions, since $\rho_i = \sqrt{\beta_i} d_i$ and the ion plasma beta, β_i , is of the order of 1 in the vicinity of 1 astronomical unit (au) (see Sec. 2 for the definitions of d_i , ρ_i , and β_i). Moreover, the radial evolution of the spectral break does not suggest any firm evidence in favor of any of the two scales (Perri et al. 2010; Bourouaine et al. 2012; Bruno & Trenchi 2014).

A recent study by Chen et al. (2014) investigated extreme regimes of β_i measured by the WIND spacecraft at 1 au, and provided a clear evidence of a beta dependence of the ion-scale break in solar wind turbulence. The main result of this study is that there is not a single scale associated to the spectral break for all values of β_i . Indeed, the spatial ion scale associated to the spectral break is observed to be always the largest of the two, namely d_i for $\beta_i \ll 1$, and ρ_i for $\beta_i \gg 1$. This suggests that the first relevant scale encountered by the turbulent fluctuations is the one that determines the transition and the properties observed in the sub-ion regime.

Numerical simulations retaining ion kinetic effects (e.g. Howes et al. 2011; Parashar et al. 2010; Passot et al. 2014; Servidio et al. 2012; Valentini et al. 2014; Cerri et al. 2016) are able to capture some of the phenomenology of the ion scale transition, leading to magnetic spectra with a steeper slope at sub-ion scales. In particular,

¹ Dipartimento di Fisica e Astronomia, Università degli Studi di Firenze, Largo E. Fermi 2, I-50125 Firenze, Italy

² INFN - Sezione di Firenze, Via G. Sansone 1, I-50019 Sesto F.no (Firenze), Italy

³ INAF - Osservatorio Astrofisico di Arcetri, Largo E. Fermi 5, I-50125 Firenze, Italy

⁴ Space and Atmospheric Physics Group, Imperial College London, London SW7 2AZ, UK

⁵ LESIA - Observatoire de Paris-Meudon, 5, place J. Janssen, F-92195 Meudon Cedex, France

⁶ Astronomical Institute, CAS, Bocni II/1401, CZ-14100 Prague, Czech Republic

RUN	$B^{\text{rms}}(B_0)$	β	$k^{\text{inj}} d_i$	$\Delta x (d_i)$	$\eta (4\pi/\omega_p)$	ppc	α_1	α_2	$k_{\perp}^b d_i$
1	0.06	1/100	0.2	0.125	5×10^{-4}	1000	-1.71	-3.52	2.89
2	0.12	1/32	0.2	0.125	5×10^{-4}	1000	-1.64	-3.53	3.47
3	0.24	1/16	0.2	0.125	5×10^{-4}	1000	-1.68	-3.22	3.46
4	0.24	1/8	0.2	0.125	5×10^{-4}	2000	-1.71	-3.22	3.41
5	0.24	1/4	0.2	0.125	5×10^{-4}	4000	-1.71	-3.06	3.01
6	0.24	1/2	0.2	0.125	5×10^{-4}	8000	-1.65	-3.00	2.55
7	0.24	1	0.2	0.125	5×10^{-4}	12000	-1.55	-2.87	2.06
8	0.24	2	0.2	0.125	5×10^{-4}	16000	-1.54	-2.87	1.90
9	0.24	4	0.2	0.125	5×10^{-4}	16000	-1.65	-2.91	1.59
10	0.48	6	0.05	0.25	1×10^{-3}	8000	-1.75	-2.91	1.09
11	0.48	8	0.05	0.25	1×10^{-3}	8000	-1.71	-3.01	1.10
12	0.48	10	0.05	0.25	1×10^{-3}	8000	-1.70	-2.99	1.01

TABLE 1
LIST OF SIMULATIONS AND THEIR RELEVANT PARAMETERS

high-resolution two-dimensional (2D) hybrid particle-in-cell (PIC) simulations by Franci et al. (2015a,b) successfully reproduce many of the observational characteristics of the transition of the turbulent cascade from MHD to kinetic scales, including a quantitative agreement of spectral slopes and compressibility and energy ratios. These works considered only one intermediate beta regime, $\beta_i = 0.5$. Different values of β_i were already investigated by means of a hybrid Vlasov-Maxwell model (Servidio et al. 2014), mainly focusing on the particle anisotropy associated to different plasma conditions. More recently, employing the same approach, Cerri et al. (2016) studied the dependence of the physics of subproton-scale kinetic turbulence on β_i by exploring three particular cases, i.e., $\beta_i = 0.2, 1$, and 5 . They observe a dominance of magnetosonic/whistler fluctuations in the low-beta case and of kinetic Alfvén waves (KAWs) in the high-beta case. The numerical study of Cerri et al. (2016) is not, however, directed to the ion spectral break as such.

In this paper we investigate the properties of turbulence and its transition from the MHD to the sub-ion regime over a very wide range of plasma betas, similar to that in Chen et al. (2014). We present a parameter study on β_i performed by means of twelve high-resolution 2D hybrid particle-in-cell simulations, focussing on the scale associated to the ion break and the steepening of the magnetic field spectrum at sub-ion scales. For extreme β_i we recover the observational results of Chen et al. (2014), whereas for intermediate cases a combination of d_i and ρ_i seems to be involved. We infer an empiric relation of the break scale as a function of β_i that provides a good fit over the whole range of values. Finally, we offer a physical interpretation of the observed phenomena.

2. NUMERICAL SETUP AND INITIAL CONDITIONS

We use the hybrid-PIC code CAMELIA (Current Advance Method Et cyclotron leApfrog), where the electrons are considered as a massless, charge-neutralizing fluid with a constant temperature, whereas the ions are described by a particle-in-cell model and are advanced by a Boris scheme. A detail description of the model equations can be found in Matthews (1994). Units of space and time are the ion (proton) inertial length, $d_i = c/\omega_p$ (ω_p being the proton plasma frequency), and the inverse proton gyrofrequency, Ω_p^{-1} , respectively. The plasma beta for a given plasma species, protons or electrons,

is $\beta_{p,e} = 8\pi n K_B T_{p,e} / B_0^2$, where $n = n_p = n_e$ is the number density, assumed to be equal for protons and electrons, B_0 the ambient magnetic field, K_B the Boltzmann constant, and $T_{p,e}$ the proton and electron temperatures. For a complete definition of all quantities, please refer to Franci et al. (2015a,b). In this paper, we present results from twelve high-resolution simulations with different values of the plasma beta, including the case already presented in Franci et al. (2015a,b). The adopted simulation box is a square grid with 2048^2 cells in the (x, y) plane. The spatial resolution, $\Delta x = \Delta y$, and consequently the box size, is not the same for all the simulations and the time step for the particle advance is adjusted proportionally. All simulations employ a few thousands of particles per cell (ppc), corresponding to many billions of particles in the whole computational grid.

The initial setup we employ here is the same as in Franci et al. (2015a,b): we initialize with an initial spectrum of magnetic and velocity fluctuations in the (x, y) plane and we impose an initial ambient magnetic field, $\mathbf{B}_0 = B_0 \mathbf{z}$, in the perpendicular direction. The initial fluctuations are composed of modes having all the same amplitude and random phases and are characterized by energy equipartition and vanishing correlation between kinetic and magnetic fluctuations. Their global amplitude, estimated as the root mean square value (rms) of the total magnetic field B computed over the whole simulation domain, B^{rms} , is not the same for all simulations. We assume that protons are initially isotropic with a given β_i . Electrons are also isotropic and their beta is always set to be $\beta_e = \beta_p$, henceforth we will simply denote the proton/electron plasma beta as β . The values of β span three full orders of magnitude, from 0.01 to 10, so that the ion inertial length, d_i , and the ion gyroradius, $\rho_i = d_i \sqrt{\beta_{\perp}}$, are well separated at the extreme values of β .

The main parameters of all the simulations are summarized in Tab. 1. In the first column we assign a number to each run, while in the next six we report, from left to right: the initial rms value of the perpendicular magnetic field, B^{rms} (in units of the ambient magnetic field, B_0), the plasma beta, β , the injection scale, $k^{\text{inj}} d_i$, i.e., the maximum scale of the initial fluctuations, the spatial resolution, Δx (in units of d_i), the value of the resistivity coefficient, η (in units of $4\pi/\omega_p$), and the number of ppc. In the last three columns we report the results of our analysis, which will be described in Sec. 3.

For larger values of β , we need to employ more ppc to keep under control the ppc-noise level at small scales, or alternatively to increase the amplitude of the initial fluctuations, B^{rms} . When β is quite low, the proton gyro-radius gets small and possibly comparable with the spatial resolution, so we need to employ smaller grid cells and the time step must be reduced accordingly. A non-zero resistivity has been introduced in order to guarantee a satisfactory conservation of the total energy, with no claim to model any realistic physical process. The resistivity coefficient, η , has been fine-tuned accordingly with the discussion presented in Franci et al. (2015b), so that the conservation of the total energy is ensured with an accuracy of less than 0.5 % for all the simulations.

3. RESULTS

All the quantities shown in the present paper are computed at the time of maximum turbulent activity, i.e., at the time when the out-of-plane component of the current density maximizes (Mininni & Pouquet 2009). The spectral properties remain quite stable afterwards (Franci et al. 2015b). The raw data (i.e., the magnetic field components) from which all the spectra were computed are available online (Franci et al. Datasets 2016), so that all the results presented here can be easily reproducible.

In the top panel of Fig. 1 we show the power spectrum of magnetic fluctuations for many different values of the plasma beta, β , versus $k_{\perp} d_i$ (for the sake of clarity, we decided not to include all the simulations here, but note that the two missing extreme cases, i.e., $\beta = 0.01$ and 10, are shown separately in Fig. 2). The spectra have been re-normalized to take into account the different amplitude of the initial fluctuations, so that they have the same power in the inertial range and can be compared more directly. All of them exhibit a power-law behavior with a Kolmogorov-like scaling in the inertial range (a $-5/3$ power law is drawn with a black dashed line as a reference), a more or less smooth break at ion scales and another power-law interval at sub-ion scales. The flattening of the spectra at higher wavevectors is not physical and only due to numerical noise. In the middle and bottom panels of the same figure, we also report all the spectra of magnetic fluctuations, compensated by $k_{\perp}^{5/3}$, as a function of $k_{\perp} d_i$ and $k_{\perp} \rho_i$, respectively. In the middle panel, all the spectra with low betas tend to overlap while the others don't, meaning that the scale of the break is fixed with d_i for $\beta \ll 1$. In the bottom panel, the opposite situation holds, i.e., all the spectra with high betas tend to overlap while the others don't, meaning that the scale of the break is fixed with ρ_i for $\beta \gg 1$. Therefore, Fig. 1 already provides a qualitative indication that the spectral break seems to be related to the larger of the two scales in both regimes, i.e., d_i for $\beta \ll 1$ and ρ_i for $\beta \gg 1$. In order to quantitatively confirm this idea, we looked at each spectrum separately and computed the break for each of them.

In Fig. 2 the spectra of the total magnetic power is reported for three representative cases: the lowest plasma beta, $\beta = 0.01$ (top panel), the intermediate value, $\beta = 1$ (middle panel), and the highest value $\beta = 10$ (bottom panel). The shape of the ion-scale break is quite different for different values of β : while it is quite sharp when $\beta \gg 1$ (bottom panel of Fig. 2), it becomes smoother

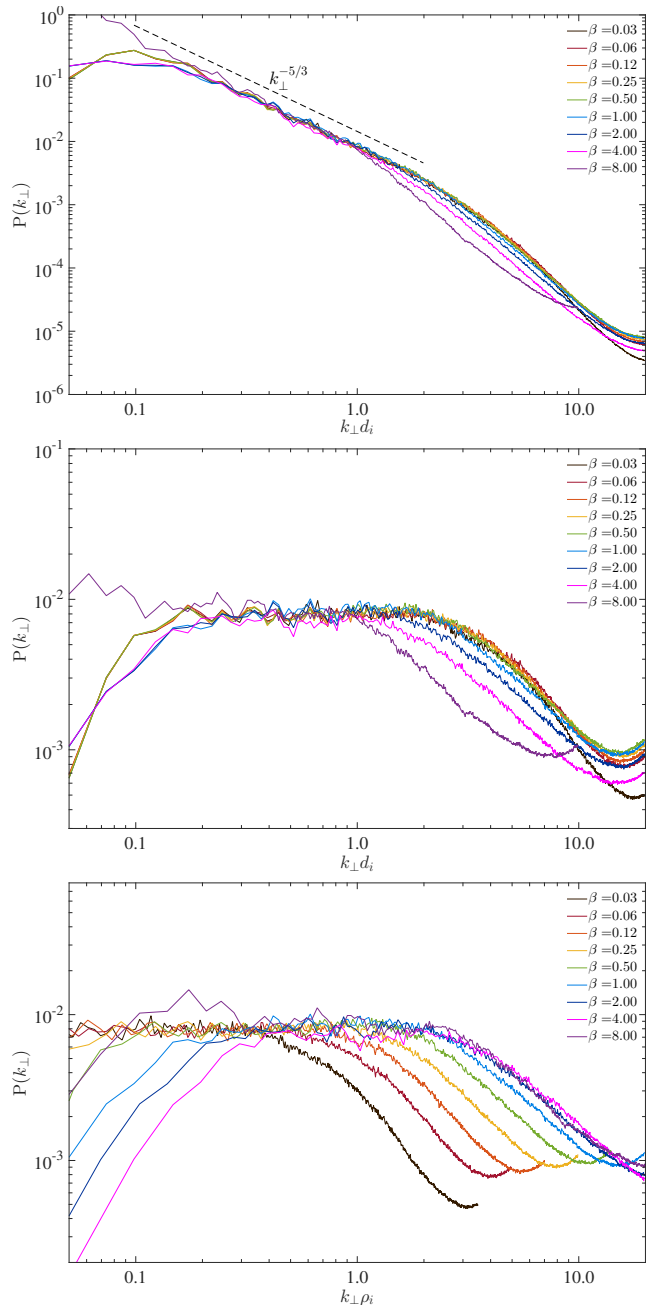


FIG. 1.— Top panel: power spectra of magnetic fluctuations for different values of the plasma beta, β , versus $k_{\perp} d_i$. Middle panel: power spectra of magnetic fluctuations for different values of β , compensated by $k_{\perp}^{5/3}$, versus $k_{\perp} d_i$. Bottom panel: the same as in the middle panel, but versus $k_{\perp} \rho_i$.

when β is low (top panel) and, in the cases with very low values determining a length scale associated to the break is not straightforward, since it might also depend on the criterion chosen to define the break itself. In order to determine such scale, we employ two different methods. The first method is the same applied by Chen et al. (2014) and we choose it in order to directly compare our numerical results with their observational data. Firstly, we compute a local power-law fit of the magnetic field spectrum over many small intervals in the range $k_{\perp} d_i \in [0.15, 15]$. The values of the local spectral index, α , for each simulation are shown in the bottom part of

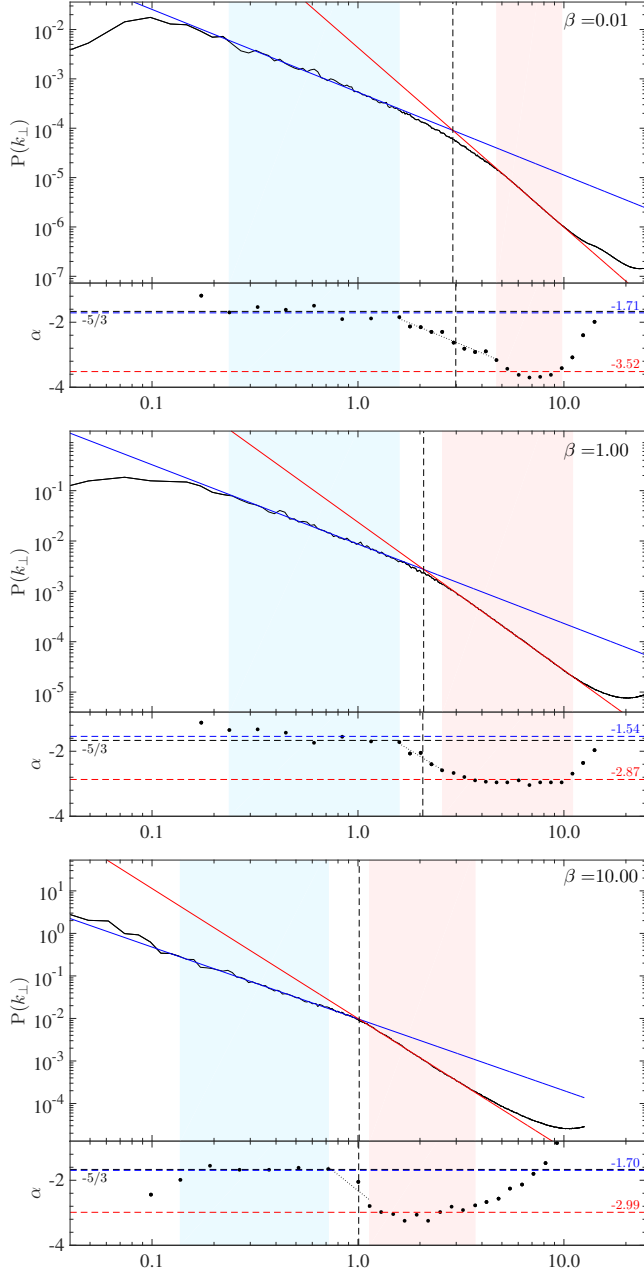


FIG. 2.— Power spectra of magnetic fluctuations for three different values of the proton plasma beta representing different regimes, i.e., $\beta = 0.01$ (top panel), $\beta = 1$ (middle panel), and $\beta = 10$ (bottom panel). The light blue and light red shaded regions mark the intervals where the global fits of the power laws were performed, for the inertial and the kinetic ranges, respectively. In the bottom parts of each panel, the value of the local spectral index, α , is also reported.

each panel of Fig. 2. We consider a range of wavevectors where α is close to $-5/3$ within a relative accuracy of $\pm 20\%$ (the light blue shaded region marks its boundaries) and we fit the values of α within this interval with an horizontal line (blue dashed line in the bottom panel), getting a value for the spectral index in the inertial range, α_1 . The sub-ion power-law index, α_2 , is determined in a similar way: we select a range of k_\perp where α is constant within a relative accuracy of $\pm 10\%$, without assuming any specific value a-priori, and we perform a fit over this

interval (indicated by a light red shaded region). Now we define the scale of the break as the wavevector at which α takes a value half way between α_1 and α_2 . The two spectral indices, α_1 and α_2 , and the scale corresponding to the spectral break, $k_\perp^b d_i$, are reported in the last three columns of Tab. 1.

In the inertial range, the power spectra of magnetic fluctuations exhibit a Kolmogorov-like behavior for all values of β , as already shown qualitatively in Fig. 1. The results of the fits for the power-law index at large scales, α_1 , are reported in Tab. 1. They are all quite close to $-5/3$, which represents the mean value, and exhibit variations of a few percent with no correlation with β . Although departures from the Kolmogorov expectation are actually observed in the solar wind (e.g., Tessein et al. 2009; Chen et al. 2013), in our simulations they seem to be mainly due to the choice of the fit interval in the inertial range, which is slightly different for each value of β (note that the break shifts towards larger scales for larger betas and the inertial range gets consequently shorter).

The results of the fits for the power-law index at sub-ion scales, α_2 , show quite larger variations, as can be seen from the second last column of Fig. 1. Indeed, α_2 is systematically less and less steep increasing the plasma beta, ranging from around -3.6 for $\beta = 0.01$ until around -2.9 for $\beta = 4$, although we observe a more general power-law spectrum with a constant spectral index ~ -2.8 for the parallel magnetic fluctuations instead (see Sec. 4). The fact that the slope increases a little bit again towards -3 for $\beta > 4$ is likely due to numerical effects: the spatial resolution, and consequently k_{\max} , is smaller and fewer particles are employed, so that the noise level at small scales is higher and this slightly affects also the slope.

While the extent of the power-law range at large scales is about a full decade for all the simulations, the one at sub-ion scales is usually smaller, being still between half a decade and a decade in most cases. In this respect, it's important to stress that, although Fig. 2 provides an insight on the whole range of β , including the extreme regimes, only the central panel is truly representative of most of the simulations in terms of the extent of power-law ranges. The other two panels allow appreciating how the method works in the worst cases, i.e., when the sub-ion range is reduced due to the shift of the break towards smaller scales (for low betas) or to the lower resolution (for large betas). Although the extent of the fit intervals at sub-ion scales is not as large as a full decade, we can still identify a power-law behavior rather than an exponential cutoff, which would be typical of resistive effects. The local spectral index α_2 is observed to be reasonably constant, with only very small variations, in the whole fit interval in all the panels of Fig. 2, especially in the middle one. The same result would not hold in the case of an exponential cut-off, since α_2 would clearly decrease before starting growing again at small scales due to numerical noise.

Alternatively, we also determined the break position by performing the global fits over the two ranges of wavevectors selected with the method explained above, plotting the straight lines which correspond to the best fit (blue and red dashed lines in Fig. 2, respectively) and determining the break as the intercept between the two. We can say a posteriori that the difference between the de-

termination of the break by the two different methods is almost negligible for all the simulations performed.

In the top panel of Fig. 3, we report the computed break scale in terms of $k_{\perp}\rho_i = 1$ (top panel) and $k_{\perp}d_i = 1$ (middle panel), as a function of β , for all the simulations performed. For $\beta \gg 1$ the points seem to settle towards an asymptotic value which is fixed in terms of ρ_i . By fitting with a straight line, we get $k_{\perp}\rho_i \sim 3$. On the contrary, when the plasma beta decreases to values $\beta \ll 1$ the points seem to approach a constant value in terms of d_i . By fitting with a straight line, we get an asymptotic value $k_{\perp}d_i \sim 3$. Since the ion inertial length and the ion gyroradius are related by $\rho_i = d_i\sqrt{\beta_{\perp}}$, we find that $d_i \gg \rho_i$ for $\beta \ll 1$ and $\rho_i \gg d_i$ for $\beta \gg 1$. Therefore, the break is found to be related to the largest of the two scales in both these separated ranges of values of the plasma beta. Differently, the spectral break does not show any clear correlation with one of the two scales when $\beta \sim 1$, meaning that it is likely related to a combination of d_i and ρ_i when they are comparable.

In the bottom panel of Fig. 3, we report the length scales associated to the break versus the plasma beta for all the simulations performed, rescaled by d_i and by ρ_i (red and blue points, respectively). We have looked for a relation $l^b = l(\beta)$ that could properly mimic the behavior of the spectral break over the whole range of values of β that we have investigated, i.e., being dimensionally correct, approaching the two asymptotic values for $\beta \ll 1$ and $\beta \gg 1$, respectively, and passing through $d_i/2 \equiv \rho_i/2$ for $\beta = 1$. The relation

$$l^b = \frac{1}{3} \left(d_i + \rho_i - \frac{\sqrt{d_i \rho_i}}{2} \right) = \frac{d_i}{3} \left(1 + \beta_{\perp}^{1/2} - \frac{\beta_{\perp}^{1/4}}{2} \right) \quad (1)$$

meets all the requirements and seems to represent quite a good approximation. In the same figure, we plot this analytical expression for l^b/d_i and l^b/ρ_i versus the plasma beta (blue and orange curves, respectively), while the black dashed line represents just a reference corresponding to the two asymptotic values $l^b/d_i = l^b/\rho_i \sim 1/3$.

4. DISCUSSION AND CONCLUSIONS

We investigated the spectral properties of plasma turbulence around ion scales, by performing 2D high-resolution hybrid particle-in-cell simulations with different values of the plasma beta from 0.01 to 10.

The total magnetic energy spectra exhibit a power-law behavior at kinetic scales with a slope varying with the plasma β . A relatively hard spectrum, with a spectral index of about -3.6 for $\beta \ll 1$, becomes less and less steep as β increases, reaching a value around -2.9 when β is of order of unity or higher (the further steepening in the power law observed for $\beta > 4$ is likely a numerical artefact due to the lower resolution and the higher noise level of those simulations). A similar, quite large variability of the spectral index of the magnetic field spectrum at sub-ion scales is also found in solar wind observations, typically between -2 and -4 (e.g., Leamon et al. 1998; Smith et al. 2006; Alexandrova et al. 2008; Bruno et al. 2014). Such spread is mainly observed in the kinetic region close to the break, i.e., in a small range of sub-ion frequencies limited to $f < 10$ Hz. Some of this large variability could

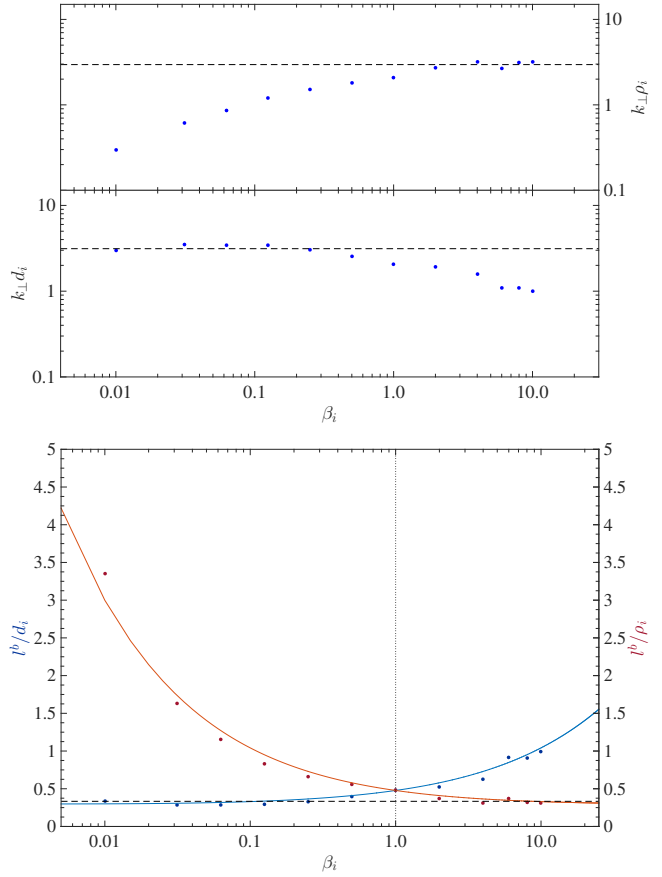


FIG. 3.— Top panel: blue points denote the wavevector k_{\perp}^b associated with the spectral break in the magnetic fluctuations, normalized to ρ_i (top half) and to d_i (bottom half), as a function of the plasma β for all the simulations performed. Dashed lines show the asymptotic values $k_{\perp}\rho_i \sim 3$ (top half) and $k_{\perp}d_i \sim 3$ (bottom half). Bottom panel: blue and red points denote the length scale l^b of the break, normalized to d_i and ρ_i , respectively, as a function of the plasma β . A blue and an orange curves represent the empirical relation $l^b = (d_i + \rho_i - \sqrt{d_i\rho_i}/2)/3$, computed in terms of d_i and ρ_i , respectively.

be related to the presence of ion instabilities or other effects (Hellinger et al. 2015; Lion et al. 2016). However, when the instrumental accuracy allows to further extend the measurement towards the electron scales, a convergence around ~ -2.8 is rather found (e.g., Alexandrova et al. 2013; Bruno et al. 2014), with a smaller variability between -2.5 and -3.1 (Sahraoui et al. 2013). Indeed, in all our simulations, a more universal power-law (e.g., independent from β) is observed for the parallel magnetic spectrum in the kinetic range, with a spectral index of -2.8 . This is clearly shown in the top panel of Fig. 4, where the power spectra of the parallel magnetic fluctuations are reported for different values of β between 1/16 and 4. Such power-law scaling is consistent with our previous simulations (Franci et al. 2015b) and with observations (Alexandrova et al. 2009). We speculate that this different behaviour of the total and parallel magnetic spectra reflects the different dependence of the compressibility on the plasma β in the inertial and kinetic range: the strong magnetic compressibility typically observed in the kinetic range (Alexandrova et al. 2008; Salem et al. 2012; Kiyani et al. 2013) is reached in a different way

from the inertial range according to its level of compressibility, i.e., the plasma β . The middle and bottom panel of Fig. 4 show that, at small scales, the perpendicular magnetic fluctuations tend to reach asymptotically the same level as their parallel counterparts. This results in the steeper power spectrum of the perpendicular (and hence, the total) magnetic field for low β , since such coupling is expected to be reached at scales smaller than the resolved ones. For high β , the level of parallel fluctuations is higher in the inertial range, so that the coupling already occurs at ion scales and the same scaling for the parallel and perpendicular power spectra is observed.

The shape of the ion-scale transition also depends on β : it is quite sharp for high values and smoother for low ones. The reason of this different behavior is not clear yet, although it could be related to the possible different nature of the processes determining the break in different regimes of β .

The associated scale-length to this break is found to be proportional to d_i for $\beta \ll 1$ and to ρ_i for $\beta \gg 1$, i.e., to the largest of the two in both limits in good agreement with solar wind turbulence at high and low beta (Chen et al. 2014). For intermediate cases, i.e., when $d_i \sim \rho_i$, a combination of the two better reproduces the scaling with β observed in our simulations. Different processes can be invoked in order to explain the position of the inertial-kinetic transition and the shape of the magnetic power spectrum at sub-ion scales. Landau damping has been considered relevant for the steepening and in introducing a non-universal power law in the magnetic spectrum (e.g., Howes et al. 2011; Passot & Sulem 2015; Sulem et al. 2016). However, in our study, the main drivers of the Landau damping (i.e., the electrons) are not treated kinetically. Alfvén waves resonances can determine the scale where the magnetic power spectrum steepens (e.g., Gary & Borovsky 2004; Bruno & Trenchi 2014; Bruno et al. 2014). However, cyclotron damping requires a significant contribution of k_{\parallel} , which is strongly inhibited in our simulations by the 2D geometry, although a local propagation of modes with $k_{\parallel} \neq 0$ can occur through the local bending of the magnetic field lines (e.g., Hellinger et al. 2015).

The transition from shear Alfvén waves to kinetic Alfvén waves (KAW) represents a possible explanation for the ion-scale break, at least when $\beta \gg 1$. This fact is corroborated by the polarizations of the fluctuations at small scales (not shown here, but the particular case with $\beta = 0.5$ was already presented in Franci et al. (2015a)), which show a good agreement with the prediction of the KAW linear theory for $\beta \gtrsim 1$ and are consistent with the fact that ρ_i is the expected scale for such transition in this regime (e.g., Chen et al. 2014). This would be consistent with the results by (Cerri et al. 2016), which observe a dominance of KAW for $\beta \gtrsim 1$ but not for lower betas.

The dispersive nature of KAW in regulating the break in the magnetic field spectrum is much more problematic when $\beta \ll 1$ since d_i , the scale we observe in this limit, seems to be relevant for KAW only under special circumstances ($T_i \ll T_e$ and for $\beta_e \gg 1$) or in presence of a large component of turbulence in k_{\parallel} (Chen et al. 2014). These conditions are not fulfilled in our simulations.

It has been suggested that the ion-scale transition

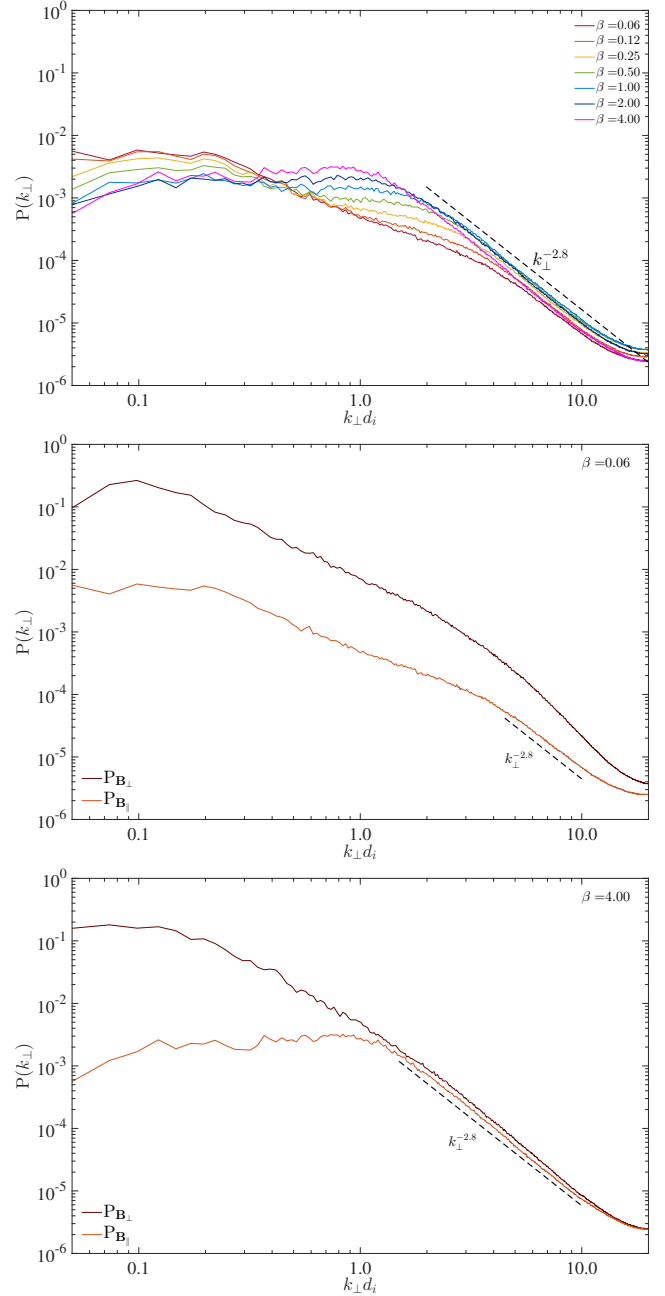


FIG. 4.— Top panel: power spectra of the parallel magnetic fluctuations for different values of β (for the sake of clarity, only the simulations with the same initial setup, i.e., the same level of initial fluctuations and the same spatial resolution, are shown here). Middle panel: comparison between the power spectra of the perpendicular and the parallel magnetic fluctuations (dark red and orange, respectively) for a low-beta case. Bottom panel: the same as in the middle panel, but for a high-beta case. In all panels, a power law with spectral index of -2.8 is reported as a reference for the scaling at sub-ion scales.

could be mainly due to the dissipation occurring in reconnecting current sheets. Indeed, the scale at which such transition occurs corresponds to the maximum in the current density spectrum, suggesting that most of current structures develops at that scale. As already shown in Fig. 2 of (Franci et al. 2015b) and therein discussed, while turbulence develops many current sheets are generated around and between coherent structures. Once formed,

these are observed to quickly disrupt due to the onset of fast reconnection. A look at the out-of-plane current density in our simulations seems to qualitatively support this interpretation: the current sheets form and shrink, and their width when reconnection occurs seems to be of the order of d_i in all simulations with $\beta < 1$ and larger when $\beta > 1$. If this process was the main responsible for the break, we would expect the associated length scale to be related to the current sheet width. Solar wind observations (Leamon et al. 2000; Vasquez et al. 2007; Borovsky & Podesta 2015) indicate that such width, although variable, scales better with d_i for $\beta < 0.1$ and with ρ_i for $\beta > 4$ (Vasquez et al. 2007). Actually, the agreement between our numerical results and (Vasquez et al. 2007) observations also extends to large betas. This could be a hint that the break might be related to reconnection for all betas. Current sheets and reconnection likely play an important role in plasma turbulence (cf., Servidio et al. 2015, and references therein).

Chen et al. (2014) pointed out that this scaling is in contradiction with results from previous simulations (Cassak et al. 2007) and laboratory measurements of reconnection with a large guide field (Egedal et al. 2007), where the current sheets thickness in the $\beta \ll 1$ condition is found to be the sound gyroradius, $\rho_s = \sqrt{T_e/T_i}\rho_i$ ($\equiv \rho_i$ when $T_e = T_i$). However, the definitions of ρ_s used in the above papers can not be easily exploited in solar wind observations, since they take into account only the reconnecting (i.e., in-plane) magnetic field.

In our simulations, the scale at which the magnetic field spectrum breaks is found to be quite well approximated by a single relation, $l^b = l(\beta_\perp)$, Eq. (1), being able to recover both the asymptotic behavior in the limits of low ($l^b \propto d_i$) and high beta ($l^b \propto \rho_i$) and the intermediate-regime scaling (a combination of the two). This relationship is qualitatively similar to that proposed by Bruno & Trenchi (2014) (basically, a mean of the d_i and ρ_i) for values $\beta \sim 1$, although here it can not be easily interpreted in terms of a resonant condition. At this level, it should be regarded as an empirical relation which can mask either a single process dominating for all betas (e.g., the current sheet width) or different processes, each one dominating at one characteristic ion scale when they are well separated and, instead, mixing in the intermediate regime (Markovskii et al. 2008), for example kinetic Alfvén waves for high β and magnetosonic-like for low β (e.g., Cerri et al. 2016).

The simulation method used in this work has a couple of limitations, i.e., the lack of electron kinetic processes and the reduced dimensionality. In the hybrid approach electrons are treated as a fluid, thus not capturing processes such as the electron Landau damping and electron kinetic instabilities. Although these processes may affect the turbulent dynamics at very small scales, possibly modifying the spectral properties in the sub-ion range, they are not expected to change the transition from large-to small-scale turbulence at ion-scales. The dissipation at the electron scales is to some extent replaced by using a finite resistivity, η . In Franci et al. (2015b), we

qualitatively checked if and how the slope in the sub-ion range is affected by η . We showed that by fine-tuning its value and controlling the scale associated to it, one can be able to separate regimes where the sub-ion spectral behavior reflects a physical cascade from cases where the change in the slope can be ascribed to purely resistive effects. Therefore, in the present work we can be reasonably confident that the sub-ion spectral slopes (where shown and discussed) are physically meaningful and indicative of a cascade process. Consistently with this, in the series of runs 3–9 we only vary β by keeping the same level of fluctuations, resolution, and resistivity, so we can exclude that steeper slopes for lower betas originate from more and more effective resistive term and claim that the systematic change in α_2 with β has a physical motivation.

The used 2D geometry allows the very high resolution and the large simulation box size needed to accurately determine the position of the ion-scale break, but the reduced dimensionality might affect the development of the turbulent cascade and of kinetic instabilities. However, preliminary 3D runs in a similar settings confirm that the perpendicular cascade is not strongly modified (see also Servidio et al. (2015)), thus suggesting that 2D simulations represent an adequate tool to investigate the spectral break.

In conclusion, our main findings about the effects of β on the magnetic field spectrum are that: i) the slope of the power law in the sub-ion range depends on β , ii) the shape and position of the ion-scale transition also depend on β , and iii) we inferred an empirical relation for the length corresponding to the ion spectral break, $l^b = [d_i + \rho_i - (d_i\rho_i)^{1/2}/2]/3$, that well describes the simulation results for all values of β .

Further investigation is needed to better clarify the nature of the ion-scale spectral break. An accurate statistical study about the current sheets thickness (e.g., Servidio et al. 2009) would allow to quantitatively investigate its scaling with the plasma beta. An analysis about the effects of β on the ion heating and temperature anisotropy and their correlation with the current density and vorticity (Servidio et al. 2015; Franci et al. 2016) will be also the subject of future work. High-resolution 3D simulations are necessary in order to extend and validate the present results.

LF is funded by the Ente Cassa di Risparmio di Firenze. PH acknowledges GACR grant 15-10057S. We acknowledge PRACE for awarding us access to resource Cartesius based in the Netherlands at SURFsara through the DECI-13 (Distributed European Computing Initiative) call (project HybTurb3D), and the CINECA award under the ISCRA initiative, for the availability of high performance computing resources and support (grants HP10C877C4 and HP10BUUOJM). Data deposit and preservation through a persistent identifier (pid) were provided by the EUDAT infrastructure (<https://www.eudat.eu/>).

REFERENCES

- Alexandrova, O., Carbone, V., Veltri, P., & Sorriso-Valvo, L. 2008, *Astrophys. J.*, 674, 1153
- Alexandrova, O., Saur, J., Lacombe, C., Mangeney, A., Mitchell, J., Schwartz, S. J., & Robert, P. 2009, *Phys. Rev. Lett.*, 103, 165003

- Alexandrova, O., Chen, C. H. K., Sorriso-Valvo, L., Horbury, T. S., & Bale, S. D. 2013, *Space Sci. Rev.*, 178, 101
- Bavassano, B., Dobrowolny, M., Mariani, F., & Ness, N. F. 1982, *J. Geophys. Res.*, 87, 3617
- Borovsky, J. E., & Podesta, J. J. 2015, *J. Geophys. Res. Space Physics*, 120, 9256
- Bourouaine, S., Alexandrova, O., Marsch, E., & Maksimovic, M. 2012, *Astrophys. J.*, 749, 102
- Bruno, R., & Carbone, V. 2013, *Living Rev. Solar Phys.*, 10, 2
- Bruno, R., & Trenchi, L. 2014, *Astrophys. J. Lett.*, 787, L24
- Bruno, R., Trenchi, L., & Telloni, D. 2014, *Astrophys. J. Lett.*, 793, L15
- Cassak, P. A., Drake, J. F., & Shay, M. A. 2007, *Phys. Plasmas*, 14, 054502
- Cerri, S. S., Califano, F., Jenko, F., Told, D., & Rincon, F. 2016, *Astrophys. J. Lett.*, 822, L12
- Chen, C. H. K., Bale, S. D., Salem, C. S., & Maruca, B. A. 2013, *Astrophys. J.*, 770, 125
- Chen, C. H. K., Leung, L., Boldyrev, S., Maruca, B. A., & Bale, S. D. 2014, *Geophys. Res. Lett.*, 41, 8081
- Egedal, J., Fox, W., Katz, N., Porkolab, M., Reim, K., & Zhang, E. 2007, *Phys. Rev. Lett.*, 98, 015003
- Franci, L., Verdini, A., Matteini, L., Landi, S., & Hellinger, P. 2015b, *Astrophys. J. Lett.*, 804, L39
- Franci, L., Landi, S., Matteini, L., Verdini, A., & Hellinger, P. 2015a, *Astrophys. J.*, 812, 21
- Franci, L., Hellinger, P., Matteini, L., Verdini, A., & Landi, S. 2016, *AIP Conf. Proc.*, 1720, 040003
- Franci, L., Landi, S., Matteini, L., Verdini, A., & Hellinger, P. 2016, EUDAT B2SHARE, pid: <http://hdl.handle.net/11304/d4c12a9e-89cb-4d67-9b51-2c9f28f52097>
- Gary, S. P., & Borovsky, J. E. 2004, *J. Geophys. Res. Space Physics*, 109, 6105
- Grappin, R., Mangeney, A., & Marsch, E. 1990, *J. Geophys. Res.*, 95, 8197
- Hellinger, P., Matteini, L., Landi, S., Verdini, A., Franci, L., & Trávníček, P. M. 2015, *Astrophys. J. Lett.*, 811, L32
- Howes, G. G., Tenborge, J. M., Dorland, W., Quataert, E., Schekochihin, A. A., Numata, R., & Tatsuno, T. 2011, *Phys. Rev. Lett.*, 107, 035004
- Kiyani, K. H., Chapman, S. C., Sahraoui, F., Hnat, B., Fauvarque, O., & Khotyaintsev, Y. V. 2013, *Astrophys. J.*, 763, 10
- Leamon, R. J., Matthaeus, W. H., Smith, C. W., Zank, G. P., Mullan, D. J., & Oughton, S. 2000, *Astrophys. J.*, 537, 1054
- Leamon, R. J., Smith, C. W., Ness, N. F., Matthaeus, W. H., & Wong, H. K. 1998, *J. Geophys. Res.*, 103, 4775
- Lion, S., Alexandrova, O., & Zaslavsky, A. 2016, *Astrophys. J.*, 824, 47
- Markovskii, S. A., Vasquez, B. J., & Smith, C. W. 2008, *Astrophys. J.*, 675, 1576
- Marsch, E., & Tu, C.-Y. 1990, *J. Geophys. Res.*, 95, 8211
- Matthews, A. P. 1994, *J. Comput. Phys.*, 112, 102
- Mininni, P. D., & Pouquet, A. 2009, *Phys. Rev. E*, 80, 025401
- Parashar, T. N., Servidio, S., Breech, B., Shay, M. A., & Matthaeus, W. H. 2010, *Phys. Plasmas*, 17, 102304
- Passot, T., Henri, P., Laveder, D., & Sulem, P.-L. 2014, *European Physical Journal D*, 68, 207
- Passot, T., & Sulem, P. L. 2015, *Astrophys. J. Lett.*, 812, L37
- Perri, S., Carbone, V., & Veltri, P. 2010, *Astrophys. J. Lett.*, 725, L52
- Sahraoui, F., Huang, S. Y., Belmont, G., Goldstein, M. L., Rétino, A., Robert, P., & De Patoul, J. 2013, *Astrophys. J.*, 777, 15
- Salem, C. S., Howes, G. G., Sundkvist, D., Bale, S. D., Chaston, C. C., Chen, C. H. K., & Mozer, F. S. 2012, *Astrophys. J. Lett.*, 745, L9
- Servidio, S., Matthaeus, W. H., Shay, M. A., Cassak, P. A., Dmitruk, P. 2009, *Phys. Rev. Lett.*, 102, 115003
- Servidio, S., Valentini, F., Califano, F., Veltri, P. 2012, *Phys. Rev. Lett.*, 108, 045001
- Servidio, S., Osman, K. T., Valentini, F., Perrone, D., Califano, F., Chapman, S., Matthaeus, W. H. 2014, *Astrophys. J. Lett.*, 781, L27
- Servidio, S., Valentini, F., Perrone, D., Greco, A., Califano, F., Matthaeus, W. H. 2015, *J. Plasma Phys.*, 81, 325810107
- Smith, C. W., Hamilton, K., Vasquez, B. J., & Leamon, R. J. 2006, *Astrophys. J. Lett.*, 645, L85
- Sulem, P. L., Passot, T., Laveder, D., & Borgogno, D. 2016, *Astrophys. J.*, 818, 66
- Tessein, J. A., Smith, C. W., MacBride, B. T., Matthaeus, W. H., Forman, M. A., & Borovsky, J. E. 2009, *Astrophys. J.*, 692, 684
- Valentini, F., Servidio, S., Perrone, D., Califano, F., Matthaeus, W. H., & Veltri, P. 2014, *Phys. Plasmas*, 21, 082307
- Vasquez, B. J., Abramenko, V. I., Haggerty, D. K., & Smith, C. W. 2007, *J. Geophys. Res. Space Physics*, 112, A11102